Towards Virtual Electrical Breast Biopsy: Space-Frequency MUSIC for Trans-Admittance Data

Bernhard Scholz

***Abstract*—Breast cancer diagnosis may be improved by electrical immittance measurements. We have developed a novel method, space-frequency *MU*ltiple *S*ignal *C*lassification (MUSIC), to determine three-dimensional positions and electrical parameters of focal lesions from multifrequency trans-admittance data recorded with a planar electrode array. A homogeneous infinite volume conductor containing focal inhomogeneities proved to be a useful patient-independent model for the breast containing focal lesions. Lesions polarized through the externally applied electric field are considered as distributions of aligned dipoles. Independence of the lesions' shape and size is achieved by a multipole expansion of such a dipole distribution. Thus, lesions are described by point-like multipoles. Their admittance contributions are given by a sum over products of multipole-specific source-sensor transfer functions, called *lead fields*, multiplied by their moments. Lesion localization corresponds to multipole search, and uses orthonormalized lead fields for comparison with a signal subspace from a singular value analysis of a space-frequency data matrix. At the locations found, the moments' frequency behavior is calculated which is assumed to be tissue-specific due to their dependence on conductivities. Results from clinical data show that space-frequency MUSIC successfully localizes lesions. Tissue differentiation might be possible, especially when the frequency range of the measurement system will be increased.**

***Index Terms*—Breast cancer, electrical bio-immittance, electrical impedance, lesion localization, MUSIC, tissue classification.**

I. Introduction

BREAST cancer is the most frequent cancer in women in the Western countries. Nearly 200 000 new cases of breast cancer are expected in the United States in 2001 [1]. In the process of diagnosis a rate of 10% of screening cases are sent to further diagnostic examinations, 25% of which have to undergo biopsy due to equivocal findings. Four out of five of these biospsies are negative [2]. In absolute figures, this means, up to 800 000 biopsies are unnecessary in the US each year. Therefore, reduction of unnecessary biopsies is mandatory. It would increase patient comfort and decrease costs.

The number of unnecessary biopsies can only be reduced by decreasing the number of equivocal findings through enhanced sensitivity and specificity. In targeted clinical studies, the admittance breast scanner TS2000[1] achieved higher rates of sensitivity and specifity when used adjunctively with X-ray mammography than mammography alone. It got FDA approval for adjunctive use with mammography. The TS2000 system will be briefly described in Section II. Despite of its success, further improvements of the TS2000 device regarding sensitivity and specificity, are desirable.

This paper presents a data model generalizing the dipole model of [4] and—based on it—presents space-frequency *MU*ltiple *S*ignal *C*lassification (MUSIC) (SF-MUSIC) as a novel method to analyze TS2000's multifrequency admittance data. MUSIC invented for the analysis of space-time data, originally in radar technology [5], then in biomagnetism [6]–[8], and in functional magnetic resonance imaging [9], is transferred to analyze space-frequency bioimmittance data.

The signal generators are supposed to be focal lesions at different positions below the measurement array having different frequency behavior of their electrical parameters. Additionally, the lesion-surrounding tissue contributes background signals over the whole measurement array of narrowly spaced 8×8 or 16×16 electrodes (interelectrode distance is 3 mm), in case of the small or the large probe. This and the spatial extension and shape of focal lesions are taken into account in the data model, see Section III. The *a priori* unknown structure of a lesion is described by a multipole expansion of a distribution of molecular and cellular dipoles in its volume.

Results of the SF-MUSIC algorithm, which will be presented in Section IV, are the three-dimensional (3-D) locations and the spectral behavior of the conductivity-dependent electrical multipole moments of possible lesions. Here and throughout this paper, conductivity means complex electrical conductivity describing conductive and capacitive tissue properties [10]. Since electrical conductivity can be assumed as tissue-specific, the frequency dependence of those moments should allow noninvasive lesion classification provided data are recorded in an appropriate frequency range. In Section V, results from clinical data are shown. They demonstrate the effectiveness of the proposed SF-MUSIC method regarding localization. They encourage measurements in an increased frequency range to establish a well-founded tissue classification procedure.

II. Measurement Device

The measurement tools are scan probes and a reference electrode. The probes contain each a planar array of electrodes (16×16 and 8×8 on the large and small probes, respectively). Each electrode has an area of 3×3 mm^2. The center-to-center distance between electrodes is 4 mm, thus leaving a space of 1 mm between adjacent electrodes. The sensing area is surrounded by a metallic strip of 7 mm width, termed the guard ring, which hinders electrical edge effects. Thus, the total probe

Manuscript received September 1, 2001; revised February 11, 2002.

The author is with the Basic Research and Development, Medical Solutions, Siemens AG, Henkestr. 127, D-91052 Erlangen, Germany (e-mail: bernhard.scholz@siemens.com).

Publisher Item Identifier 10.1109/TMI.2002.800609.

[1]TransScan TS2000 (TransScan Medical, Ltd., Migdal Ha'Emek, Israel) is the medical industry's first commercially available electrical immittance scanner.

Fig. 1. Breast examination with the TransScan TS2000 breast scanner. The patient lies recumbent, holding the cylindric reference electrode in the hand contralateral to the examined breast.

areas are 79×79 mm^2 and 47×47 mm^2 of large and small, respectively. The reference electrode is a metallic cylinder (diameter: 3.4 cm; length: 12 cm) which is held by the patient in her hand, Fig. 1.

Current flow through the breast is induced by a potential difference between probe electrodes being at ground potential, and the reference electrode. The potential of the reference electrode is adjusted automatically such that the current signals are optimal. Safety regulations limit the voltage to 2.5 V and the current to 5 mA. The TS2000 currently operates with up to 30 voltage frequencies in the range from 58 Hz to 5 kHz.

For each sensor, signal amplitude and phase shift are derived from the current data measured during recording time [4]. These quantities are converted into admittances, which are visualized as maps over the electrode array. Actually, grey scale maps of conductances and capacitances are displayed.

III. Breast and Lesion Model

The breast containing focal lesions is considered as a homogeneous volume conductor except for the regions of the lesions. They are assumed to have different electrical conductivity than the surrounding. The volume conductor is supposed to be of infinite extent. This means, boundary influences are assumed to be negligible which has been verified by clinical data analysis, so far. Thus, the breast model is completely patient-independent.

In absence of conductivity inhomogeneities, the electric field in such a breast model is homogeneous provided the external field sources are far away. In a lesion-less case, this picture of a homogeneous electric field also applies to the breast region below the planar TS2000 measurement array due to a uniform potential across this array and a reference potential in the contralateral hand of the patient [4]. The electric field is directed normal to the measurement array.

In the presence of lesions, the externally applied electric field polarizes the lesion due to conductivity differences of the lesion (κ_L) and the surrounding breast tissue (κ_B). Permanent and induced dipoles are oriented along this electric field. Therefore, a lesion is a region of aligned dipoles. It can be considered as an externally induced and as a spatially extended source of an electrical polarization field. The aim of this section is to express the admittance measured through lesion-specific quantities describing the polarization field.

The polarization field of a cancerous lesion with higher conductivity than the surrounding tissue, e.g., a cancerous lesion, enhances the current flow along the applied electric field inside and outside the lesion where it is decreasing with distance. Depending on its distance with respect to the measurement grid, and on its size, shape, and orientation, the lesion is detectable through increased current signals [12].

The total current density $\vec{j}$ is a sum of the current densitiy $\vec{j}_A$ due to the externally applied field $\vec{E}_A$, and of the lesion-induced polarization current density $\vec{j}_L$. It can be related to the potential of the polarization field.

$$\vec{j}(\vec{r}) = \vec{j}_A + \vec{j}_L = \vec{j}_A - \kappa_B \vec{\nabla} \phi_L(\vec{r}). \tag{1}$$

The applied electric field and the measured currents are ac quantities of a definite, but adjustable frequency. In the subsequent text, electric field and currents stand always for the respective amplitude quantities. Due to the electric properties of tissue, the currents measured depend on the frequency of the applied electric field.

The admittance Y_m measured at the mth electrode (position vector $\vec{r}_m$) is determined by the component of the total current density normal to the electrode surface. Since the measurement array is planar, all normals are equal, and—without loss of generality—are assumed to direct into z-direction. Therefore, we have

$$Y_m(f) = \frac{A_{\text{Electrode}}}{U} \vec{e}_z \bullet \vec{j}(\vec{r}_m, f) \quad m = 1, \ldots, M \tag{2}$$

where M is the total number of electrodes, $A_{\text{Electrode}}$ the area of each electrode, U the potential difference between measurement array and reference electrode, f the frequency of the applied voltage, and $\vec{e}_z$ the unit vector in z direction.

Since size and shape of the lesions are unknown, a possible way of data description is to get rid of the explicit dependence on their geometry. This is achievable by a multipole expansion of the distribution of the aligned dipoles.

The electrical potential ϕ_L at position $\vec{r}$ due to an arbitrary distribution of elemental dipoles in a lesion of volume $V(\vec{r}' \in V)$ within an infinite volume conductor, is given by

$$\phi_L(\vec{r}, f) = -\frac{1}{4\pi\kappa_B} \int_V d\vec{r}\,' \vec{p}(\vec{r}\,', f) \bullet \vec{\nabla} \frac{1}{|\vec{r} - \vec{r}_{\text{CoGL}} - \vec{r}\,'|} \tag{3}$$

where

f	frequency of the externally applied electric field;
$\vec{p}(\vec{r}\,', f)$	frequency-dependent elemental dipole moment density;
$\vec{r}_{\text{CoGL}}$	center-of-gravity (CoG) of the lesion of volume V;
$\vec{\nabla}$	Nabla operator acting on the position vector $\vec{r}$.

More precisely, $\vec{p}$ is a current dipole density. By writing $\vec{p} = i\omega\ \vec{m}$ and using $\kappa = i\varepsilon_0\varepsilon$ (ε_0: permittivity of vacuum), we obtain a potential expression with permittivity and standard dipole density replacing conductivity and current dipole density. Therefore, description in terms of current dipoles or in terms of harmonically varying electric dipoles is equivalent. We continue the discussion with the current dipole density without using explicitly the term "current dipole," later on.

As can be seen from (3), the tissue-specific frequency dependence of the lesion signal is now ascribed to the frequency behavior of the elemental dipoles. In (3), dipole–dipole interactions within V are assumed to be considered by ascribing an effective polarizability to each elemental dipole [13]. The expression in (3) can be generalized to multiple lesions by summing over all existing polarized regions. The interactions between separated polarized regions will be neglected [14]. For the sake of notational clarity we continue with a *single* lesion.

The multipole expansion of (3) up to third-order with respect to the CoG of the lesion yields the following expression

$$\phi_L(\vec{r},f) = -\frac{1}{4\pi\kappa_B}\left\{\vec{d}(f)\bullet\vec{\nabla} - \underline{\underline{q}}(f)\bullet\vec{\nabla}\otimes\vec{\nabla} + \frac{1}{2}\underline{\underline{\underline{k}}}(f)\bullet\vec{\nabla}\otimes\vec{\nabla}\otimes\vec{\nabla} + \cdots\right\}\frac{1}{|\vec{r}-\vec{r}_{\mathrm{CoGL}}|} \quad (4)$$

where the $\otimes$ denotes the tensor product, and the big dot means complete contraction of all vector or tensor indexes, respectively. The first term of (4)—the monopole term of the expansion of a dipole distribution—is the overall dipole moment of the lesion, denoted as $\vec{d}$. The second term has a quadrupolar structure, and the third term is of octupolar type. In general, the multipole nature of the contributions of (4) is augmented by one, compared with a corresponding expansion of a charge distribution. The potential can be thought of as being generated by *point-like* moments located at the lesion's CoG. They are given by

$$\vec{d} = \int_V d\vec{r}'\vec{p}(\vec{r}'), \quad \underline{\underline{q}} = \int_V d\vec{r}'\vec{r}'\otimes\vec{p}(\vec{r}')$$

and

$$\underline{\underline{\underline{k}}} = \int_V d\vec{r}'\vec{r}'\otimes\vec{r}'\otimes\vec{p}(\vec{r}'). \quad (5)$$

The dependence on the lesion's geometry has disappeared at the expense of a series of terms. In (4) and (5), the CoG as the location of the point-like moments and the frequency are omitted in order to facilitate readability.

The multipole structure of (4) becomes similar to that of a charge distribution, if the alignment of the dipoles is taken into account. As assumed above, the externally applied electrical field and the elemental dipole moment vectors are oriented along the z direction. Thus, the dipole moment density is $\vec{p} = p\vec{e}_z$, and has only a single nonvanishing component. It can be considered henceforth—like a charge density—as a scalar. Considering in (4) the orientations described, calculating the gradient of the potential, and inserting the result into (1), and then inserting the current density expression into (2), we get for the admittance measured at the mth electrode position at frequency f

$$Y_m(f) = \frac{A_{\mathrm{Electrode}}}{U}\times\left\{\vec{e}_z\bullet\vec{j}_A(\vec{r}_m,f) + L_1(\vec{r}_m,\vec{r}_{\mathrm{CoGL}})d(f) + \vec{L}_2(\vec{r}_m,\vec{r}_{\mathrm{CoGL}})\bullet\vec{q}(f) + \underline{\underline{\underline{L}}}_3(\vec{r}_m,\vec{r}_{\mathrm{CoGL}})\bullet\underline{\underline{t}}(f) + \cdots\right\}. \quad (6)$$

Equation (6) expresses the admittance in terms of the "background" current density j_A and in terms of geometrical and electrical multipole quantities L_1, $\vec{L}_2$, $\underline{\underline{\underline{L}}}_3$, d, $\vec{q}$, and $\underline{\underline{t}}$ describing a lesion with CoG at position $\vec{r}_{\mathrm{CoGL}}$ and a frequency-dependent strength. Thus, lesions are considered as multipolar signal sources, in addition to the inevitable "background" signals from surrounding breast tissue. Subsequently, the multipole quantities are discussed.

The tensor rank of the moments, compared with (5), is reduced by one. The total scalar dipole moment d of the lesion is given by

$$\vec{d}(f) = \vec{e}_z d(f) = \vec{e}_z\int_V d\vec{r}'p(\vec{r}',f). \quad (7)$$

The quadrupole moment reduced to a vector is

$$\underline{\underline{q}}(f) = \int_V d\vec{r}'\vec{r}'p(\vec{r}',f)\otimes\vec{e}_z \equiv \vec{q}(f)\otimes\vec{e}_z. \quad (8)$$

In case of a homogeneous spherical dipole distribution, the reduced quadrupole moment is zero, as is easily seen and as it should be. The second-rank tensor $\underline{\underline{t}}$ is defined by

$$\underline{\underline{t}} = 3\underline{\underline{l}} - \mathrm{trace}(\underline{\underline{l}})1_3 \quad (9)$$

where 1_3 is the 3-D unit tensor, and $\underline{\underline{l}}$ is related to the octupole moment $\underline{\underline{\underline{k}}}$ of (5) via

$$\underline{\underline{\underline{k}}}(f) = \int_V d\vec{r}'\vec{r}'\otimes\vec{r}'p(\vec{r}',f)\otimes\vec{e}_z \equiv \underline{\underline{l}}(f)\otimes\vec{e}_z. \quad (10)$$

As mentioned above, the elemental dipoles are assumed to be frequency dependent in a tissue-specific way. Through the multipole expansion, this frequency dependence is adopted by the multipole moments, see (7)–(10). Thus, the frequency dependence of the admittance, initially given by the elemental dipoles, is now explained by the frequency behavior of the multipole moments. Further, their in- and out-of-phase parts, i.e., their real and imaginary parts, are related to real and imaginary part of the admittance data.

The source-electrode-dependent functions L_1, $\vec{L}_2$, and $\underline{\underline{\underline{L}}}_3$ give rise to maps specific for each point-like multipole moment, Fig. 2. Following bioelectricity [15] and biomagnetism [16], they are called *lead fields*. From the multipole expansion up to

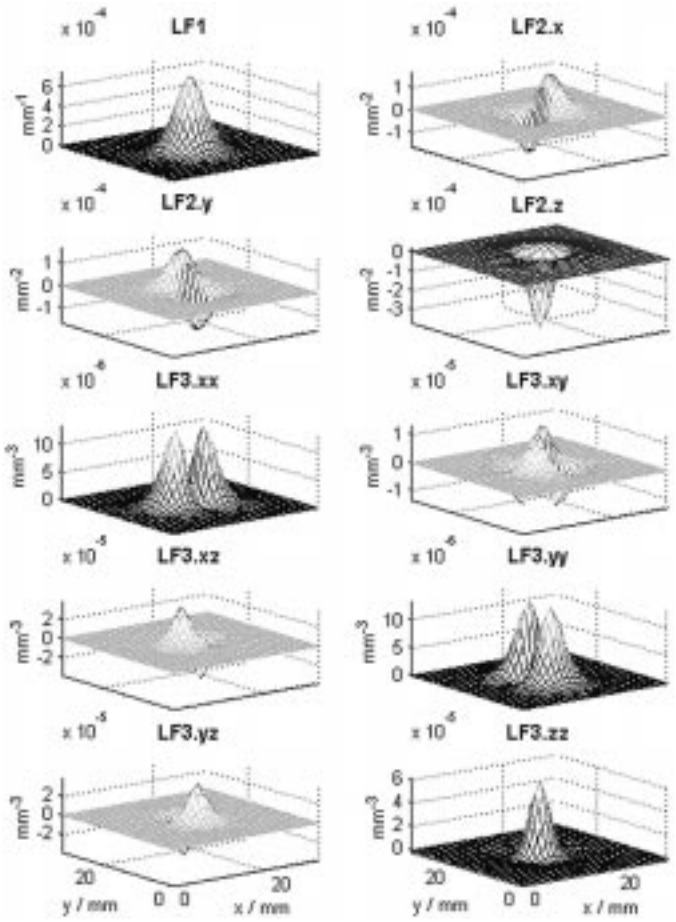

Fig. 2. Multipole lead fields of a source in a depth of 6 mm. LF1: dipole lead field; LF2: vectorial quadrupole lead field; LF3: tensorial octupole lead field, according to the first, second, and third term of the multipole expansion of a distribution of aligned dipoles (see text).

third-order of a focal distribution of *aligned* dipoles, we have a single dipole, three quadrupole, and six octupole lead fields.

The first lead field L_1 is a scalar field due to the scalar dipole moment (7). Correspondingly, the vector nature of $\vec{L}_2$ is related to the reduction of the quadrupole moment to a vector (8), and the second-rank tensor property of $\underline{\underline{L}}_3$ is a consequence of the reduction of the octupole moment to such a tensor.

The complexity of their map structure increases with multipole order, Fig. 2. The z component lead fields (LF1, LF2.z, and LF3.zz) describe the symmetric shape of a lesion signal. Asymmetry is modeled by the other lead fields. Thus, linear combination of maps from multipole lead fields increasing with order, allows description of data maps of increasingly complicated structure caused by shape and size of a lesion.

From (6) it can be seen that the lead fields define a model subspace of the M-dimensional (M-D) data space. This model subspace depends on the multipole source position, thus describing the fact that the admittance data depend on the position of the lesion.

The admittance expression in (6) can be generalized to multiple lesions by summing over the different CoGs and the associated multipole moments. This generalization will be presented in Section IV-D. There, the spectral behavior of the multipole moments will be determined by inverting the set of linear equations relating measured admittances and the multipole moments from different lesions.

IV. Space-Frequency MUSIC

The problem to be solved in this work, is the 3-D localization of focal lesions, and subsequently the estimation of the spectral behavior of the localized lesions, in order to diagnose their benign or malignant nature. The mathematical structure of this localization problem is the same as that used to estimate the directions of arrival of wavefronts impinging onto a sensor array in radar measurements, or to estimate the three-dimensional positions of focal brain activities in magnetoencephalographic measurements. In these applications, spatio-temporal data, recorded with a sensor array at different time instants, are used to derive a signal subspace of the data space. At each point within the volume-of-interest, a measure of orthogonality between this signal subspace and an application-specific model subspace is calculated. The peaks of the three-dimensional distribution of measures are identified as source locations. At the positions located, the source strengths as a function of time are calculated by inverting the set of linear equations relating the measured data and the source strengths.

A. Space-Frequency Data Matrix

Given the breast and lesion model of Section III, it is obvious to analyze space-frequency admittance data with the MUSIC algorithm. Therefore, the SF-MUSIC method requires TS2000 admittance maps at different frequencies $f_n, (n = 1, \ldots, N)$. The maps are reformatted as M-D column vectors $\underline{Y}$ in order to define a $M \times N$ space-frequency data matrix $\boldsymbol{Y}$ of measured admittances

$$\boldsymbol{Y} \equiv (\underline{Y}(f_1), \ldots, \underline{Y}(f_N). \tag{11}$$

The column vectors characterized by simple underline, are defined as

$$\underline{Y}(f_n) = (Y_1(f_n), \ldots, Y_M(f_n))^T. \tag{12}$$

The underline is also used later in the text and has the meaning as in (12). Note, the matrix $\boldsymbol{Y}$ is a complex matrix. In case of conductance or susceptance data only, the matrix in (11) will be real.

B. Singular Value Decomposition

The number of sources, i.e., of lesions, is supposed to be extractable from a singular-value decomposition (SVD) of $\boldsymbol{Y}$. This assumes, lesions with perfectly coherent frequency behavior signal generators are not present. The SVD is

$$\boldsymbol{Y} = \sum_{k=1}^{\min(M,N)} s_k \, \underline{u}_k \otimes \underset{\sim}{v}_k^T \tag{13}$$

where s_k are the real singular values, and $\underline{u}_k$ and $\underset{\sim}{v}_k$ are M-D and N-dimensional (N-D) unitary vectors, respectively [17], being orthonormalized vectors in case of real matrices. The

M-D vectors $\underline{u}_k$ depend on spatial, i.e., electrode position indexes, only. If reformatted two-dimensionally, they can be displayed as maps like the original data. They form a set of basis vectors of the complex data space. The frequency dependence is contained in the N-D vectors $\overset{v}{\sim}_k$. It should be noted, that the vectors $\underline{u}_k$ and $\overset{v}{\sim}_k$ are dimensionless, and that singular values have the dimension of the measured data.

The number of *numerically significant* singular values is related to sources behaving linearly independently with frequency. This behavior is determined by the *polarizability* of the source regions, which in turn depend on both, the conductivities of the polarized regions and those of the surroundings. For a sphere the polarizability is known to be proportional to $(\kappa_L - \kappa_B)/(\kappa_L + 2\kappa_B)$. E.g., the frequency behavior of signals from two spherical lesions can differ in case of equal lesion conductivities but different conductivities of the surroundings.

The basis vectors related to the significant singular values are called signal *eigenmaps*, and show regular structures determined by signals from the background tissue, and from lesions, if present. They span the so-called *signal subspace*. The residual maps are eigenmaps, which are mostly determined by noise, and they define the *orthogonal* signal subspace.

C. Localization

Based on the data model presented, localization of focal lesions corresponds to find point-like multipoles by comparing the signal subspace with the position-dependent lead field or model subspace in the volume conductor. The first steps of a search procedure are discretization of the search volume, and evaluation of a localization function, localizer for short, at each grid point. Depending on the type of localizer, its minima or maxima, respectively, are interpreted as CoGs of lesions.

The localizer proposed here and most approved with clinical data, uese uses lead fields $\underline{U}_{L,p}, (p = 1, \ldots, P)$ which are derived from the $P = 10$ lead fields L_1, $\vec{L}_2$, and $\underline{\underline{L}}_3$ of Section III. The steps of derivation are first normalization and second orthogonalization. The initial normalization compensates the decrease of higher order multipole fields with increasing distance from the measurement array: map structures of such lead fields are considered taken into account at all positions. Additionally, normalized lead fields are dimensionless: lead fields of different multipole orders are treated on equal footing. Recall, the basis vectors of the signal subspace and its orthogonal compliment are also dimensionless. Next, the orthogonalization leads to lead fields with a mixed multipole structure as real lesion are supposed to have. These orthogonalized lead fields $\underline{U}_{L,p}(\vec{r})$ also depend on the position $\vec{r}$ of the point-like multipoles as the original lead fields do. They can be regarded as test fields corresponding to possible lesions at the position under consideration.

At each grid point $\vec{r}$, the P orthogonalized lead fields $\underline{U}_{L,p}(\vec{r})$ are tried to be expressed in a least squares sense in terms of the S eigenmaps. This allows defining cost functions F_p as

$$F_p(\vec{r}) = \left| \sum_{s=1}^{S} c_s \underline{u}_s - \underline{U}_{L,p}(\vec{r}) \right|^2 \quad \text{with } p = 1, \ldots, P. \tag{14}$$

The $\underline{U}_{L,p}$ with the best fit determines the value of the localizer F. This means

$$F(\vec{r}) = \min_{\{\forall\, p\}} \left\{ 1 - \sum_{s=1}^{S} \left(\underline{u}_s^H \cdot \underline{U}_{L,p}(\vec{r}) \right)^2 \right\}, \text{ with } p = 1, \ldots, P. \tag{15}$$

The H in (15) denotes Hermitian conjugation of the complex eigenmaps. Using the projector $\boldsymbol{P} = 1 - \sum_{s=1}^{S} \underline{u}_s \otimes \underline{u}_s^H$, we see that (15) corresponds to a measure of orthogonality onto the orthogonal signal subspace. We get

$$F(\vec{r}) = \min_{\{\forall\, p\}} \left\{ \left| \boldsymbol{P} \underline{U}_{L,p}(\vec{r}) \right|^2 \right\}. \tag{16}$$

In the presence of lesions and under the assumption that model errors are tolerable, this measure exhibits *local minima*. They are identified as CoGs of the lesions.

Since lesions give rise to peaks in an admittance map, the search can be restricted to a line search below the peaks into depth direction. This procedure corresponds to the picture of an *algorithmic needle* inserted into a virtual breast.

In case of several focal lesions with linearly independent frequency behavior, the localizer is expected to have the corresponding number of local minima.

D. Multipole Spectroscopy and Tissue Classification

The frequency courses of the lesions' multipole moments are assumed to be tissue-specific, see Section III. They are calculated by inverting the linear relation between the measured admittances and the moments at the positions of the lesions located.

This inversion requires the localization result, since the position vector of the lesion has to be inserted into the lead fields of (6).In case of several localized lesions, the contributions from moments at all locations are considered by summing over all localized positions. The multiple lesion version of (6) will now be given in matrix form in order to discuss the inversion for lesion sources at multiple locations. The $M \times P$ single source lead field matrix (P: number of lead fields; $\vec{r}$: source location) is defined as

$$\boldsymbol{L}(\vec{r}) = \left(\underline{L}_1(\vec{r}), \underline{L}_{2,x}(\vec{r}), \ldots, \underline{L}_{3,xx}(\vec{r}), \ldots, \underline{L}_{3,zz}(\vec{r}) \right). \tag{17}$$

As before, see (12), the underline denotes a M-D vector in data space. The multipole expansion up to third-order of Section III has yielded ten lead fields. The ten source and frequency-dependent moments, (7)–(9), are collected into a column vector (f: frequency)

$$\boldsymbol{m}(\vec{r}, f) = \left(d(\vec{r}, f), q_x(\vec{r}, f), \ldots, t_{xx}(\vec{r}, f), \ldots, t_{zz}(\vec{r}, f) \right)^T. \tag{18}$$

The extension to Q localized lesions, requires a multiple source lead field matrix $\boldsymbol{\Lambda}$. Its dimensions are $M \times Q \cdot P$

$$\boldsymbol{\Lambda} = \left(\boldsymbol{L}(\vec{r}_1) \ldots L(\vec{r}_Q) \right). \tag{19}$$

Correspondingly, the multiple source moment vector is a $Q \cdot P$-dimensional column vector

$$\boldsymbol{\mu} = (\boldsymbol{m}(\vec{r}_1) \ldots \boldsymbol{m}(\vec{r}_Q))^T . \tag{20}$$

For each frequency f, we get from the multiple lesion version of (6), the following relation between the admittances and the multipole moments of Q localized lesions

$$\underline{Y}(f) = \frac{A_{\text{Electrode}}}{U} [\underline{1} \quad \boldsymbol{\Lambda}] \begin{pmatrix} j_{A,z}(f) \\ \boldsymbol{\mu}(f) \end{pmatrix} \tag{21}$$

where $\underline{1}$ is M-D column vector with ones as components, and $j_{A,z}$ denotes the z component of the background current density. The ones-column appears because a homogeneous background current density $j_{A,z}$ across the measurement array is assumed.

The frequency dependence of the moments is now calculated by solving (21) at all measured frequencies. The solution is obtained by a generalized inversion of (21). Due to the complex nature of admittance, the moments and the background current density are complex, too. Thus, their real and imaginary parts, or their magnitudes and phases are subject to further analyses.

V. Results

SF-MUSIC has been applied to clinical TS2000 data. The frequency range was between 100 Hz and 5 kHz, and the number of frequencies varied between four and seven. The data have been recorded without knowledge of any further data analysis. Therefore, edge artifacts due to bad probe-breast contact have occurred in several cases. They have been removed in a preprocessing step. The same holds for boundary data due to probe movements while measuring. Otherwise, they introduce artificial frequency dependence. Too noisy data, up to now only measured in the low-frequency range from 100 Hz to 2 kHz, have been excluded from the study.

A first analysis involved 41 data sets from histologically proven cases. All lesions besides three benign ones, could be localized. The depth positions from line searches below peaks were compared with the CoG depths determined by ultrasound. The differences have been smaller than half of the lesions' extension in depth direction. This means, the SF-MUSIC locations have been found to be always within the lesions' volumes as determined by ultrasound.

The localization results are suitably assessed and visualized by means of a normalized localization error. It is defined as the difference between the ultrasonic CoG depth z_{CoG} and the depth localized z_{loc} divided by half of the lesion's depth extension h_{Lesion}, i.e., $\varepsilon = 2(z_{\text{CoG}} - z_{\text{loc}})/h_{\text{Lesion}}$. Positions found within the lesions' volumes have ε values between -1 and $+1$. With the direction of increasing depth as positive z direction, positive ε values are related to positions localized between the measurement array and the ultrasonically determined CoG depth, whereas negative values are from positions found in a depth greater than the "ultrasonic" CoG depth.

The plots in Figs. 3 and 4 show, the localization results do not depend on the depths and the volumes of the lesions, as known from ultrasound. However, notice, the volumes have been of moderate size. The three outliers, i.e., the positions found outside the lesions' volume are from benign cases. Since the aim of the localization method is to find malignant lesions, and all of them have been found, these three results are not considered as serious.

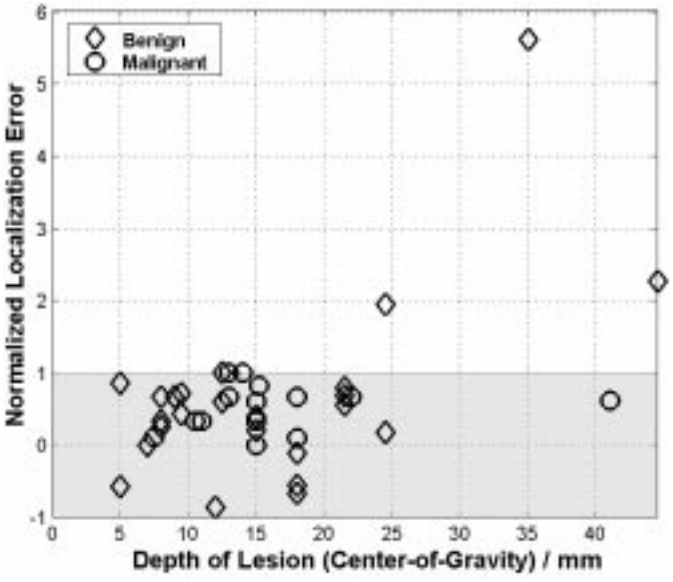

Fig. 3. Normalized localization error of the search results versus the depth of the lesion as determined by ultrasound. Localizations within the lesions' volume are within the shadowed region (see text).

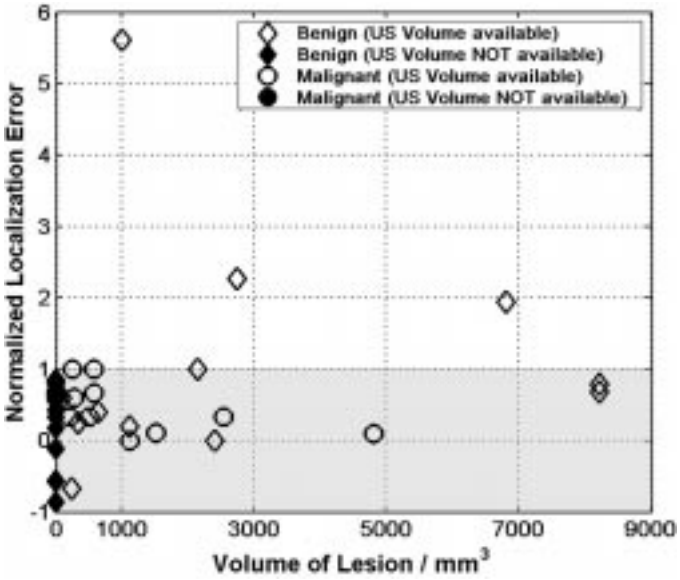

Fig. 4. Normalized localization error of the search results versus the volume of the lesion as determined by ultrasound. Localizations within the lesions' volume are within the shadowed region (see text).

As an example of a SF-MUSIC application, results from data generated by a cancerous lesion in a depth of 13 mm are presented. The preprocessed conductance maps are shown in Fig. 5. From single focal lesion data, Fig. 5, two significant singular values and two signal eigenmaps are expected due to two tissue components leading to signals with linearly independent frequency behavior: the lesion and the surrounding tissue, Fig. 6. The eigenmaps are shown in Fig. 7.

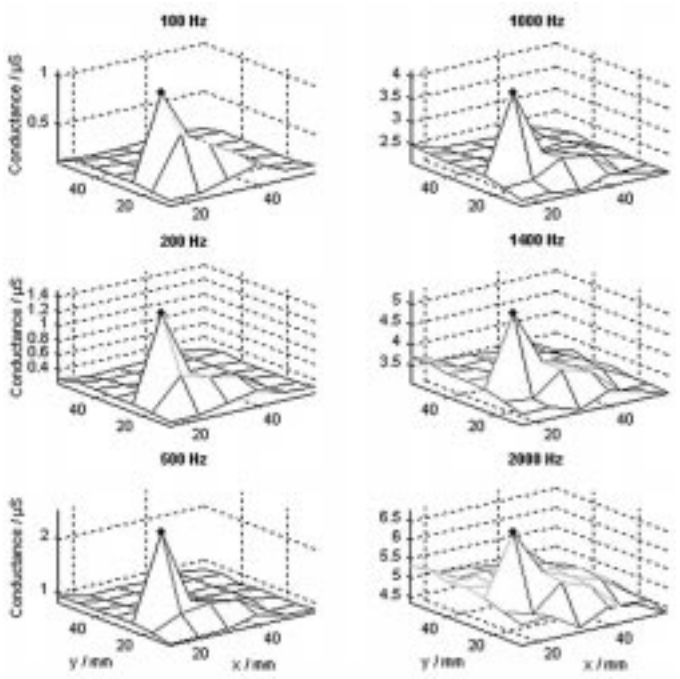

Fig. 5. Multifrequency TS 2000 conductance data from a malignant lesion. Its depth is 13 mm, and its spatial extensions are 12, 8, and 6 mm in x, y, and z direction , as determined by ultrasound. Boundary artifacts are removed.

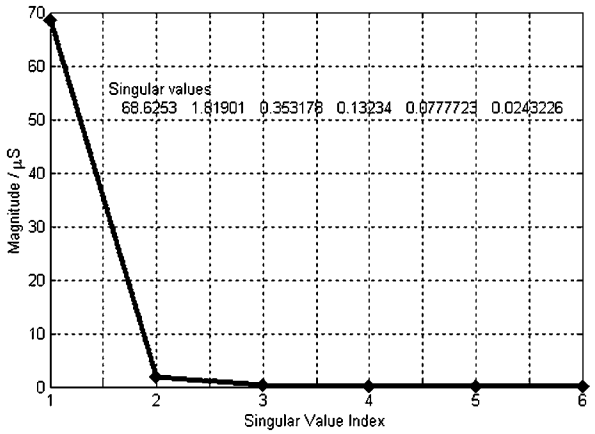

Fig. 6. Singular value spectrum of admittance data, the real part of which is shown in Fig. 5. There are two significant singular values.

A line search below the peak signal yielded the cost function of Fig. 8. It shows a local minimum at a depth of 11 mm which is within the lesion as determined by ultrasound. The localized CoGs differ by 2 mm only, the normalized localization error is +2/3.

At the location found, the frequency behavior of the complex multipole moments can be calculated according to Section IV-D. A discussion of moment-versus-frequency curves is meaningful only if curves from *large* set of patient data of the *same* histology would be available. The number of patient data analyzed up to now, is too low to show representative curves and to draw statistically significant conclusions. Therefore, display of such curves is omitted.

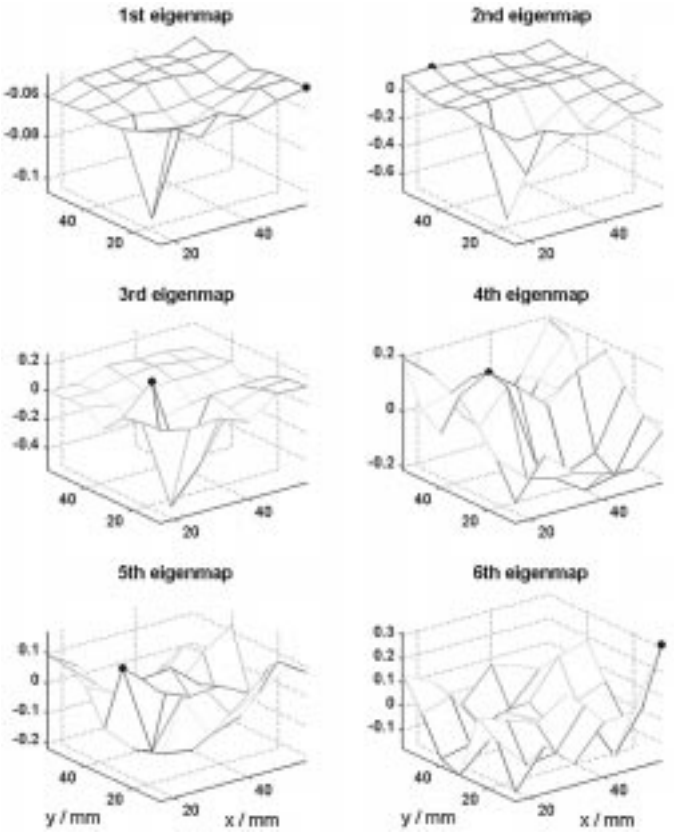

Fig. 7. The real eigenmaps from the SVD of the data displayed in Fig. 5. The first two eigenmaps are considered as basis vectors of the signal subspace.

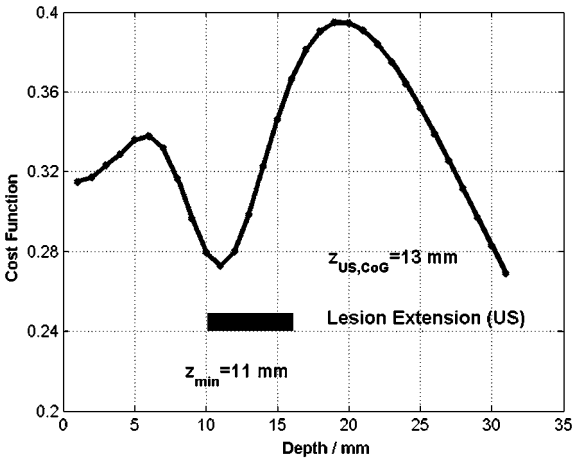

Fig. 8. Cost function of the localizer defined in Section IV-C for the admittance data of Fig. 5.

VI. Discussion

The MUSIC method was transferred and adapted to the analysis of multielectrode and multifrequency admittance data from the breast recorded with the TS2000 system. The goal has been to present an algorithmic tool which will allow decision whether admittance data are generated by benign or malignant lesions. Since the SF-MUSIC line search for lesions can be imagined as conduction of an algorithmic needle, the term *virtual electrical biopsy* seems appropriate.

The immediate results of SF-MUSIC are 3-D positions of focal lesions, and the frequency behavior of electrical parameters. In this version of the algorithm these parameters are multipole moments. Since they depend on the lesions' conductivities, a tissue-specific frequency behavior can be expected.

The first action in SF-MUSIC is extraction of the number of conductivity regions and definition of the signal subspace through an SVD of the space-frequency data matrix. This requires that both, the polarizabilities of the lesions and the conductivity of the tissue surrounding the lesions, behave linearly independent with frequency. Multifocal lesions with identical frequency behavior of their signals will be detectable in a future version of this SF-MUSIC part.

Localization of the lesions, is the second step and is a precondition for calculation of the multipole moments. Inputs are the signal subspace and the lead fields as model maps from sources modeling the lesions. These maps are *patient-independent* and the sources, the multipoles, are point-like. Therefore, they are independent of the unknown size and shape of the lesions. Size and shape are shifted to the moments of the multipoles. This description has been obtained from a multipole expansion of a distribution of aligned dipoles representing the lesion, within an infinite volume conductor representing the breast. The successful localizations of lesions from patient data suggest that this patient-independent breast model and the lesion model are justified, at least for the medium-sized lesions investigated so far.

In the case of artifact-free data, localization errors less than half of the lesions' depth extension, indicate that model errors are small. This is certainly also related to the design of the TS2000 measurement probe. Within the ultrasound and TS2000 measurement errors, the locations from both methods agree. Also, the orthogonal lead field localizer has turned out to be superior to other localizers. Taking the maximum principal angle [18] between the signal and the lead field subspaces as a localizer, outliers have occurred. Likewise, the projection localizers from biomagnetism [6] have yielded too much inacceptable results. In investigating localizers it has been advantageous not to incorporate an expression for the background field.

Up to now, multipole moments have been calculated for a too small number of clinical data. Additionally, they have been measured in the probably too restricted frequency range between 100 Hz and 5 kHz. Measurements including frequencies of the β-dispersion range [10] up to some megahertz, are expected to lead to moments from which the tissue-specific behavior can be better observed or deduced. This expectation is based on the conductivity measurements of various types of breast tissue [19], [20]. Future research should include a statistically sufficient number of patients in order to be able to draw diagnostically relevant conclusions.

In summary, in this paper, a physically consistent and a mathematically transparent approach toward virtual electrical breast biopsy has been proposed.

ACKNOWLEDGMENT

The author would like to thank Prof. Kaiser and Dr. A. Malich, Institute of Diagnostic and Interventional Radiology, University of Jena, Jena, Germany, for the patient data, He would also like to thank R. Anderson, now with Siemens Medical Solutions, Concord, CA, for managing the necessary contacts and data exchanges.

REFERENCES

[1] Statistics web page, American Cancer Society, Inc., http://www3.cancer.org/cancerinfo, Aug. 2001.
[2] Web page describing, "Breast cancer diagnosis," Imaginis Corporation, Cary, NC, http://www.imaginis.com/breasthealth, Aug. 2001.
[3] "Transcan T-Scan 2000 gets panel nod as mammography adjunct," *Gray Sheet, Med. Devices, Diagnostics Instrum.*, vol. 24, no. 34, pp. 5–6, 1998.
[4] M. Assenheimer, O. Laver-Moskovitz, D. Malonek, D. Manor, U. Nahaliel, R. Nitzan, and A. Saad, "The T-Scan technology: Electrical impedance as a diagnostic tool for breast cancer detection," *Physiol. Meas.*, vol. 22, no. 1, pp. 1–8, 2001.
[5] R. O. Schmidt, "Multiple emitter location and parameter estimation," *IEEE Trans. Antennas Propagat.*, vol. AP-34, pp. 276–280, Mar. 1986.
[6] J. C. Mosher, P. S. Lewis, and R. M. Leahy, "Multiple dipole modeling and spatio-temporal MEG data," *IEEE Trans. Biomed. Eng.*, vol. 39, pp. 541–557, June 1992.
[7] A. Oppelt, R. Graumann, and B. Scholz, "Zur magnetischen Ortung bioelektrischer Quellen, Teil 1: Ortung einzelner und mehrerer Stromdipole," *Z. Med. Phys.*, vol. 3, pp. 59–63, 1993.
[8] T. Elbert, M. Junghöfer, B. Scholz, and S. Schneider, "The separation of overlapping neuromagnetic sources in first and second somatosensory cortices," *Brain Topogr.*, vol. 7, no. 4, pp. 275–282, 1995.
[9] K. Sekihara and H. Koizumi, "Detecting cortical activities from fMRI time-course data using the MUSIC algorithm with forward and backward covariance averaging," *Magn. Reson. Med.*, vol. 35, pp. 807–813, 1996.
[10] S. Grimnes and O. G. Martinsen, *Bioimpedance & Bioelectricity Basics*. San Diego, CA: Academic, 2000.
[11] J. D. Jackson, *Classical Electrodynamics*, 2nd ed. New York: Wiley, 1975.
[12] B. Scholz and R. Anderson, "On electrical impedance scanning—Principles and simulations," *electromedica*, vol. 68, pp. 35–44, 2000.
[13] C. J. F. Boettcher, *Theory of Electric Polarization*. Amsterdam, The Netherlands: Elsevier Scientific, 1973.
[14] H. A. Pohl, *Dielectrophoresis*. Cambridge, U.K.: Cambridge Univ. Press, 1978.
[15] R. Plonsey and R. C. Barr, *Bioelectricty*. New York: Plenum, 1988.
[16] J. Sarvas, "Basic mathematical and electromagnetic concepts of the biomagnetic inverse problem," *Phys. Med. Biol.*, vol. 32, no. 1, pp. 11–22, 1987.
[17] E. Anderson, Z. Bai, C. Bischof, S. Blackford, J. Demmel, J. Dongarra, J. Du Croz, A. Greenbaum, S. Hammarling, A. McKenney, and D. Sorensen, *Lapack Users' Guide*, 3rd ed. Philadelphia, PA: SIAM, 1999.
[18] G. Golub and Ch. Van Loan, *Matrix Computations*, 3rd ed. Baltimore, MD: The Johns Hopkins Univ. Press, 1996.
[19] J. Jossinet, "Variability of impedivity in normal and pathological breast tissue," *Med. Biol. Eng. Comput.*, vol. 34, pp. 346–350, 1996.
[20] ——, "The impedivity of freshly excised human breast tissue," *Physiol. Meas.*, vol. 19, pp. 61–75, 1998.